Seasonal variations of river and tidal flow interactions in a tropical estuarine system

Preprint *in* Continental Shelf Research · September 2019

DOI: 10.1016/j.csr.2019.103965

Jorge Zavala-Hidalgo
Universidad Nacional Autónoma de México

Erick Olvera
Universidad Nacional Autónoma de México

Journal Pre-proof

Seasonal variations of river and tidal flow interactions in a tropical estuarine system

L. Tenorio-Fernandez, J. Zavala-Hidalgo, E.R. Olvera-Prado

PII: S0278-4343(19)30348-6

DOI: https://doi.org/10.1016/j.csr.2019.103965

Reference: CSR 103965

To appear in: *Continental Shelf Research*

Received Date: 28 December 2018

Revised Date: 26 July 2019

Accepted Date: 30 August 2019

Please cite this article as: Tenorio-Fernandez, L, Zavala-Hidalgo, J, Olvera-Prado, E.R, Seasonal variations of river and tidal flow interactions in a tropical estuarine system, *Continental Shelf Research*, https://doi.org/10.1016/j.csr.2019.103965.

Seasonal variations of river and tidal flow interactions in a tropical estuarine system

Tenorio-Fernandez L[1]., Zavala-Hidalgo J[2]., Olvera-Prado E. R[2,3].

[1] Centro Interdisciplinario de Ciencias Marinas del Instituto Politécnico Nacional - CONACyT, México. [2]Centro de Ciencias de la Atmósfera, Universidad Nacional Autónoma de México, México.

[3]Center for Ocean-Atmospheric Prediction Studies, Florida State University.

Corresponding author: Leonardo Tenorio-Fernandez

E-mail: leonardo.tenof@gmail.com / ltenorio@ipn.mx

Continental Shelf Research
July 2019

1. Abstract

The tidal hydrodynamics of a tropical estuarine system with river outflow seasonal variations was studied. Water level observations from eleven sites within the system were analyzed over one year in a restricted and shallow tropical estuary. The analysis was performed using wavelets, power spectral density analysis and a linear analytical model. This methodology gives the principal tidal components, their amplitude, phase and the interactions between the tide and the seasonal variations of the river outflow. The analytical model included the river discharge as an extra force on the frictional parameter to help understand the seasonal variations in tidal propagation within an estuary. The system was divided into three zones based on its bathymetry, geometry and river influence. Each zone presented different seasonal responses. River influence showed a 30% decrease in the

amplitude of tidal signal from the mouth to the head, and the hydrodynamics were driven by the balance between the pressure gradient and frictional forces. This high tide attenuation in the river influence zone showed seasonal variations, therefore this research proposes adding into the frictional forces the river discharge to the frictional parameter in the analytical solution. The results show that although river discharge has a marked sub-tidal periodicity, river discharge has a strong influence on tidal hydrodynamics and inhibits the propagation of the tide toward the head of highly frictional estuarine systems.

2. Introduction

In estuaries, the periodic variations of hydrographic variables and currents can be classified into intratidal and subtidal according to their frequency. The intratidal variations correspond to periods of less than 25 hours and the phenomena that produce them are diverse; the most common example of these processes is the astronomical tide, with semidiurnal (~12 hours) and diurnal (~24 hours) periods. Subtidal variations, on the other hand, have lower than diurnal frequencies, as the result of various processes, such as those related to the tidal amplitude variations over periods of 13 to 15 days or 27 to 31 days, or those caused by atmospheric phenomena lasting 3 to 10 days due to the atmospheric forcing in the synoptic scale. Additionally, there are other subtidal variations associated with the inflow of freshwater from rivers and rainfall. The flow or the circulation associated with these variations are also known as residual circulation or residual flows (Jay, 2010).

In coastal bodies of water such as estuaries, the circulation induced by tides may play a key role in controlling the system hydrodynamics, as well as the exchange with the adjacent ocean (Winant, 2007). The variations in water surface levels in estuaries or coastal lagoons are better understood by exploring the tidal and subtidal dynamics and their relationship with other forces such as friction and the flow of river discharge. When the tide propagates across these systems, its amplitude can either increase or decrease. The rate of change of tidal amplitude and its phase depends on the geometry and friction of the system, river discharge, wave height within the system, upwelling-induced sea level, and above all, the frequency of the type of harmonic components entering the system (LeBlond, 1978; Friedrichs, 2010; Sassi and Hoitinnk, 2013; Tenorio-Fernandez *et al.,* 2016).

Restricted, choked, branched and shallow coastal lagoons and estuaries are usually highly frictional, and consequently the frictional forces have significant weight in the hydrodynamic balance. When the tidal signal is propagated, it is strongly attenuated within the lagoon due to frictional forces (Tenorio-Fernandez *et al.,* 2016). Winant (2007) has proposed an analytical model to describe the propagation of the tide in elongated systems; this model (2007) is helpful because it uses an arbitrary cross-section, resolving both the amplitude and phase within the system. The solution of the model can be used in coastal systems, estuaries, and coastal lagoons. It demonstrates that in highly frictional systems, the tidal amplitude decreases exponentially from the mouth to the head, so that the model solution is described by the balance between the pressure gradient and frictional forces (Tenorio-Fernandez *et al.,* 2016). This solution is a function of two dimensionless parameters, namely frictional and geometric (Waterhause et al., 2011); although the analytical solution of Winant (2007) did not consider the influence of the river, it can be included in the frictional parameter (Godin, 1999).

In estuaries, variations in water surface levels can be modified by river discharge. At the mouth of estuaries and coastal lagoons, the tidal flow is generally several times higher than the average flow from the river, and hence water surface level variations are mainly controlled by tides in areas close to the mouth. The dominance of tides decreases with the distance from the mouth, and river discharge becomes the key driver in controlling variations in surface water (Sassi and Hoitinnk, 2013). This research aims to describe the tidal hydrodynamics and its interaction with rivers in a branched tropical system that includes a zone without river influence, on the western side, and an estuarine environment fed by two rivers on the eastern side. The working hypothesis is that the tidal signal on the side without river influence (western) may be represented by an exponential wave that decreases as a consequence of the geometry of the basin alone, which favors increased friction. On the river influence zone (eastern side), the exponential decay waveform that represents the propagation of the tide decreases due to the combined effect of the geometry of the basin and the flow from the rivers, which is considered in the frictional parameter in the analytical model and this parameter shows a seasonal variation.

3. Study Area

This study was carried out in the Alvarado-Papaloapan system, located along the southwestern coastline of the Gulf of Mexico. It is a combined system, that comprises the Alvarado coastal lagoon to the west and the estuary formed by the Limón and Papaloapan rivers to the east (Fig. 1). The inflow of freshwater from both rivers is the main factor that influences the longitudinal density gradient. The Papaloapan river supplies the greatest flow of water. According to its geomorphological origin, this system can be classified as a sand barrier estuary (Valle-Levinson, 2010; Olvera-Prado, 2014).

The Alvarado-Papaloapan system is located within 18°36' - 18°54' N, and 96°00' - 95°30' W, covering an area of 46 500 km^2 and with a mean annual rainfall above 1800 mm. It is Mexico's second most important river system, after the Grijalva-Usumacinta system. The Alvarado-Papaloapan system communicates with the sea through a mouth, with a width of approximately 1.1 km and a maximum depth of 18 m. The main tidal components in the adjacent sea of the system are lunisolar (K_1), diurnal lunar (O_1) and the main semidiurnal lunar (M_2), it is forced through its mouth by the mixed tide with a diurnal predominance regime (Kantha, 2005) and the tidal range is approximately 80 cm (Olvera-Prado, 2014).

The Alvarado-Papaloapan hydrological system is composed mainly of the Papaloapan river as mainstream to the east, with an average annual flow rate of 650 m^3/s; Limón river, with an average annual flow rate of 68 m^3/s; and on the west side of the system, the Alvarado zone system has an extension of approximately 85 km^2 from mouth to head and it communicates with the Camaronera lagoon through natural channels (Fig 1). All these characteristics confer a high complexity to the Alvarado-Papaloapan system, making it hydrodynamically appealing.

The Alvarado-Papaloapan system was divided according to its hydrodynamic characteristics into the Alvarado zone, including the Camaronera Lagoon; the Limón river zone; and Papaloapan river zone (Fig. 1). The Alvarado zone was designated A, B, C, D, E, measuring stations, the Limón river zone was designated G, H and L measuring stations and in the Papaloapan river zone there was only I measuring station, J was the mouth measuring station and K was not included in the analysis (Fig. 1).

4. Collection data and methodology

Measurements of the water surface level were recorded in 11 sites from the mouth of the estuary to its heads (Laguna Camaronera, Limón river, and Papaloapan river) from August 2011 to September 2012 (approximately one year in all cases, except for the sensor anchored at the mouth), to obtain a complete description of tidal propagation. Recording period, depth and location of each sensor is shown in Table 1. The pressure sensors used were U20-001-01 Titanium HOBO Water Level data logger, with an accuracy of ~0.5 hPa equivalent to 0.5 cm; these sensors were set to take readings at 15-minute intervals. The data recorded provided information on the free surface elevation, in centimeters, in Greenwich Mean Time (GMT). The flow rate of the Papaloapan and Limón rivers were obtained from the hydrometric stations of the National Register of Surface Waters, which is part of the National Hydrometric Network (Olvera-Prado, 2014).

This spatial arrangement of instruments allowed for a complete measurement of the variations of water level within the system, from the mouth to the heads. The harmonic analysis proposed by Pawlowicz *et al.* (2002) was applied to all time series of water surface levels recorded with pressure sensors. The amplitude and phase of the tide for the main constituents were obtained using the least squares method, which included a Rayleigth criterion of 1 and a nodal correction. The uncertainty of the tidal constituents was calculated using the signal-to-noise ratio (snr), which relates the original signal to the noise signal (Pawlowicz et al., 2002). Once the main tidal constituents were known, the tide was characterized by the form number (F), defined as $F = (K_1 + O_1) / (M_2 + S_2)$ (Defant, 1958).

The contribution of the tide to the total variation of water surface level variability was quantified using the coefficient of determination (R^2) as the explained variance, defined as:

$$R^2 = \left[1 - \frac{Var_{res}}{Var_{tot}}\right] \times 100 = \left[1 - \frac{\sum_{i=1}^{n}\left(E_{ti} - M_{pi}\right)^2}{\sum_{i=1}^{n}(Et_i)^2}\right] \times 100,$$

where n is the total number of data, Var_{res} is the variance of the estimated residuals, *i.e.*, the sum of squared differences in total elevation E_{ti} minus expected tide M_{pi}, and Var_{tot} is the sum of the squared total elevation variance E_t.

Once the percent of variance due to the astronomical tide was determined, the spectrum analysis (wavelet analysis and power spectrum density) was applied. The wavelet analysis provided the highest energy period over time and locates the fluctuations of energy in the time series, in this case water level time series (Torrence and Compo, 1998). In addition, the power spectrum density (PSD) was calculated for each series (Emery and Thomson, 2001).

Based on the observations, the amplitude and phase of the principal tidal components were determined for each site; however, the amplitude and phase along the longitudinal axis are not known. To this end, a linear model was used to describe the tidal evolution in a semi-enclosed, elongated lagoon system, with an arbitrary cross-section (bathymetry), and constant turbulent viscosity and density. This linear model assumes the hydrostatic approximation and considers as boundary conditions the non-displacement one at the bottom, and the kinematic one at the surface. The linear solution of the lowest order proposed by Winant (2007) was applied for the analysis of the propagation of the tidal wave in gulfs (Winant, 2007) and in elongated estuaries (Waterhouse *et al.*, 2011; Henrie and Valle-Levinson, 2014).

This solution is based on two additional parameters: δ and κ. The former is the frictional parameter δ, which relates friction to local acceleration (it is an approximation of the Stokes number) and is determined as $\delta = (2K^*/\omega^* H^{*2})^{\frac{1}{2}}$ (Winant, 2007). Hereinafter dimensional variables are represented with an asterisk,

K^* is turbulent viscosity, ω^* is frequency of the tide, and H^* is an average depth. The latter κ is the geometric parameter, which represents the relative importance between the length of the water body and the length of the tidal wave, defined as $\kappa = \omega^* L^*/(g^* H^*)^{\frac{1}{2}}$,, where g^* is gravitational acceleration and L^* is the length of the water body. The solution in the one-dimensional lowest order (longitudinal axis) for the variations of sea surface elevation ($N^{(0)}$) (Winant, 2007), which meets the boundary conditions, is given by

$$N^{(0)} = \frac{cos[\kappa\mu(1-x)]}{cos(\kappa\mu)} \tag{1}$$

$N^{(0)}$ being a complex number that represents the standardized amplitude and the phase of the variations of water surface level; μ is also a complex number in terms of δ, κ; and f, the last parameter is the Coriolis dimensionless parameter, $f = f^*/\omega^*$, and f^* is the Coriolis parameter. The standardized position along the longitudinal axis x ranges from 0 to 1, where zero is the mouth and one is the maximum length of the water body. For further details on the calculation of μ, refer to Winant (2007).

Since the study area shows the characteristics of a highly frictional lagoon and estuary (Tenorio-Fernandez *et al.,* 2016; Waterhouse *et al.,* 2011), the previous solution in equation (1) changes because the tidal signal decreases exponentially toward the end of axis x (Winant, 2007). Therefore, the equation for the propagation ($N^{(0)}$) of the tidal wave in highly frictional water bodies is defined as:

$$N^{(0)} = exp[-(1+i)\kappa\delta\gamma x] \tag{2}$$

where the parameter γ is of order 1 and depends on the geometry of the water body (Winant, 2007). Equation (2), which describes the variations of surface water level along axis x has been used in other investigations (Van Rijn, 2011a; Waterhouse et al., 2011; Tenorio-Fernández *et al.,* 2016). The whole description of the lower order solution can be found in Winant (2007).

The amplitudes and phases obtained with equation (2) for the main diurnal and semidiurnal tidal harmonics O_1 and M_2 along axis x were compared with the amplitudes and phases observed. However, to determine the temporal variations of both amplitude and phase, the measurement period was divided into bimonthly sub-periods, and a harmonic analysis and the analytical solution were conducted for each sub-period. Those series from which data are missing for any two-month period were excluded from this analysis.

5. Results

5.1 Water surface level

We obtained 11 time series of sea level variations corresponding to the different stations. For a better visualization, only one complete cycle of spring and neap tides is shown for each zone (Alvarado zone, Papaloapan river zone and Limón river zone, Fig. 2 top panel, middle panel and bottom panel), *i.e.*, a 30-day period, as an example of the time series of water surface elevation. The phase lag with respect to the J station is evident in all the figures, as well as the attenuation and the distortion of the tidal signal toward the heads (A, I and L stations), the variations due to astronomical forcing and those that do not depend on these. The greatest amplitude in the daily tidal range was recorded at the J station in spring tides, with an average range of ~0.8 m and in the neap tides of ~0.3 m. During neap tides, in the Papaloapan river zone the mean tidal range is ~0.25 m; and in the Alvarado zone is ~0.23 m. While during spring tides, in both zones, the mean tidal ranges is ~0.60 cm. The smallest amplitudes were observed in A and L stations, where mean tidal ranges are ~0.07 m in neap tides meanwhile in spring tides did not exceed 0.20 m.

The spectral analysis (the wavelet analysis and the power spectrum density) for each signal and each station is shown in Fig. 3 to 6. Note that in these figures each wavelets x-axis has a different time axis length because the pressure time series doesn't have the same time period. The wavelet of the J station shows three distinct energy peaks that fluctuate through time (Fig. 3). The first corresponds to the diurnal band, with a period approaching 24 hours; the second, of higher energy, corresponds to low frequencies with periods of more than 24 hours (not discussed here); and the third in importance is the semidiurnal band, with a period of 12 hours. The peaks that correspond to tidal bands are directly related to astronomical forcings, and the harmonic analysis reveals that the main tidal components are O_1 and K_1 for the diurnal signal, and M_2 and N_2 for the semidiurnal signal. The low frequencies are principally related to fortnightly periods corresponding to the spring and neap tides and during the neap tides, the semidiurnal energy increases (see Fig. 3).

Within the system, in the Alvarado zone, the amplitude of the diurnal and semidiurnal variations are reduced as the tidal signal travels to the estuary head (Fig. 4). The energy corresponding to semidiurnal periods in station A disappears, while the diurnal energy, although very low, still persists at the far edge of the Alvarado zone (Fig. 4 station A). In the Limón river zone, although with lower energy, the energy profiles at station H resemble the ones at the J station (Fig. 5). This is due to the closeness of the two stations; as the tide moves away from the J station toward station L, the energy related to semidiurnal and diurnal frequencies decreases significantly, to the extent that the semidiurnal energy virtually dissipated and the diurnal energy becomes extremely low at the station L (Fig. 5). In August and September 2011, and in June, July and August 2012 (coinciding with the wet season), the energy of diurnal and semidiurnal frequencies either dissipates or becomes imperceptible in the L station (Fig. 5). And in the Papaloapan river zone, the diurnal band shows a well-defined energy peak, which is the most important one (Fig. 6). However, even though station I is the closest to the station J, the energy in the band corresponding to the semidiurnal period is low (Fig. 6, bottom panel), and practically disappeared in September 2011 and August 2012 (Fig. 6b).

The coefficient of determination, R^2, indicates that in most stations the dominant phenomenon that affects the variations of sea surface elevation is the astronomical tide (Table 2). In station H, station I and J station, and Alvarado zone stations B, D, and E, R^2 is higher than or close to 60%, since these are the sites closest to the sea and, therefore, are most influenced by tides. In Limón river stations, G, K and L, the coefficient of determination R^2 is approximately 50%, and in A station it is 30%. These stations, which showed the lowest coefficient, indicate that other processes that contribute to the fluctuations of the surface elevation become more important and the tides contribute 50% or less (Table 2).

From the harmonic analysis, the amplitude and phase of the main tidal components were obtained for each site (Table 2). From the mouth to the heads, the constituents with the greatest amplitude are the diurnal constituents K_1 and O_1, with no significant difference in their importance across the lagoon-estuary complex. The semidiurnal component of greatest importance is M_2, with greater amplitude than N_2 throughout the basin. According to the form number (F), the dominant tidal regime observed in the entire system is diurnal, except at the mouth, where the regime is mixed-mainly diurnal, which means that the tide loses its mixed characteristic as it propagates into the estuary. At the mouth the tide has diurnal amplitude of ~13 cm and a semidiurnal, M2, of ~ 7.8 cm; both are attenuated as the signal propagates toward the heads of the basin.

In the Alvarado zone, the diurnal signal is attenuated by 24% to station B (far edge of the lagoon) and by 84% to the far edge of station A. In the Limón river zone, the diurnal tide signal is attenuated by 84% to station L; in the Papaloapan, the attenuation is 17% to station I. The semidiurnal signal is the one that experiences the greatest attenuation toward the head, being undetectable by sensors placed at the head of the Alvarado zone, station A and the head of the Limón river zone, station L. In the Papaloapan river zone, the M_2 semidiurnal signal is attenuated by 18% at station I, and the N_2 signal by 28%. All attenuation percentages of the main tidal components are relative to the corresponding amplitude at the station J.

Using the phase lags of the tidal components relative to the station J, the delay of tidal signals was calculated for the stations farthest away from the station J. The diurnal signal takes ~2 hours to travel from the station J to station B and ~6 hours to reach the farthest point, station A; the semidiurnal signal takes ~1 hour to reach station B and does not reach station A because it is completely attenuated. In the

Limón river zone, the diurnal signal is delayed by ~6 hours from J to L stations and the semidiurnal signal is no longer detectable at station L. In the Papaloapan river zone, the diurnal signal takes ~1 hour to reach station I, and the semidiurnal signal takes ~0.8 hours to reach this same station.

These results clearly show that the hydrodynamics of the Alvarado-Papaloapan system is consistent with a highly frictional system in all zones. Both the diurnal and semidiurnal signals are attenuated along each zone within the system, with the semidiurnal signal being completely dissipated at the heads of the Alvarado zone and Limón river zones. This attenuation reaches its peak level in August and September in both the diurnal and semidiurnal signals, particularly at the head of Limón, station I and station L. It is also in these months that the Papaloapan river and the tributaries of the Limón river contribute the highest water flow (top panel of Fig. 5 and 6).

5.2 Analytical Model

The wavelet analysis revealed that the attenuations of tidal components show spatial and temporal differences, and the months with higher attenuation in both diurnal and semidiurnal signals are those with the highest effluent by the rivers (May to October). Hence, it is demonstrated that the interaction between the tide and the inflow from rivers plays a key role in the system, at least in their respective areas of influence. Therefore, the methodology proposed by Tenorio-Fernández *et al.,* (2016) is used for the bimonthly description of the tidal propagation along the longitudinal axis. Following Henrie and Valle-Levinson (2014), the model of Winant (2007) was applied by zone in the Alvarado-Papaloapan lagoon-estuarine system. The large attenuation percentages are indicative of a highly frictional estuarine system. Therefore, equation (2) is the solution used, with the parameter δ being the term associated with attenuation; the analytical solutions are fit to the observations obtaining the propagation of the bimonthly tidal signal and, therefore, the seasonal variations in parameter δ. It is noted that the analytical model fits the observations, the analytical solution satisfactorily resolves the amplitude of the dominant tidal harmonics and the analytical phase solutions are good approximations of the observed phases (Fig. 7 and Fig. 8).

Alvarado zone. This analysis does not consider station A, i.e. the solution and fitting of the tidal propagation are applied to station B, since the morphological restrictions between Alvarado zone and Laguna Camaronera become complex and increase frictional forces (Fig. 7a, 7d and Fig 8a, 8d). Alvarado zone behaves as a highly frictional water body, where the balance between the pressure gradient and frictional forces control the tidal hydrodynamics. The highest attenuations along the longitudinal axis occur in the semidiurnal signal (Fig. 8a); however, the main diurnal and semidiurnal components remain significant at station B (Fig. 7a and Fig. 8a). The phase lag analytical solutions are sub-estimated for both tidal components and during all months. The maximum phase lag obtained by the analytical model between the B and J station is in agreement with the observations (Fig. 7d and Fig. 8d); the phase lags obtained are $\sim$1.5 hours for the diurnal and semidiurnal signals. The values of parameter δ do not show a significant seasonal variation for either the diurnal or the semidiurnal signals (Fig. 7a and Fig. 8a); however, the biggest values of this parameter for diurnal signals are in May, June, July and August, for the semidiurnal are in July and August, leading to biggest attenuations and phases lags of these tidal components (Fig. 7a and Fig. 8a).

Papaloapan river zone. The measurement and analysis in this zone are characterized by a single sensor in the Papaloapan river, not too far from the influence of the adjacent ocean, unfortunately one sensor that was deployed farther out of the mouth was lost. The Papaloapan zone has the biggest seasonal variation of the frictional parameter (δ), in July, August, September and October the attenuations of both signals are higher compared to other months of the year (Fig. 7b and Fig. 8b). With the semidiurnal signal displaying the greatest attenuations during these months. During this period the Papaloapan river discharge is high (Fig. 7b and Fig. 8b). July, August, September and October analytical solutions of the diurnal and semidiurnal phase lags are a good approximation of the observations, the remaining months are sub-estimated with respect to the measurements phase lags in both signals. The maximum phase lag obtained from the analytical model between the I and J station is ~25° (0.9 hours) for the diurnal signal and ~30° (1 hour) for the semidiurnal signal, which results in a delay similar to the one observed, *i.e.* ~1.5 hour for the diurnal signal and ~1 hours for the semidiurnal signal (Fig. 7e and Fig. 8e).

Limón river zone. Station K was not considered in the analysis, since it is located outside of the channel fed by the Limón river. In the Limón river zone, the main tidal components are attenuated from the mouth to the most remote station. The frictional parameter (δ) has monthly variations, the highest values of these parameters are between May and October for diurnal and semidiurnal signals, therefore the biggest attenuation in Limón river zone are in the months of highest Limón river discharge (Fig. 7c and Fig. 8c). The diurnal signal is the only one that is significant at station L, although from July to October it is almost imperceptible. While between May and August the semidiurnal signals are statistically imperceptible or completely attenuated at the most remote station (Fig. 7c and Fig. 8c). The phase lag obtained from the analytical model for the diurnal signal from the mouth to station L is ~120°, causing a delay of ~8 hours in the signal (Fig. 7f).

6. Discussion

The tidal influence on the coastal system depends of the adjacent sea tidal characteristics. The main tidal components in the Gulf of Mexico are lunisolar (K_1), diurnal lunar (O_1) and the main semidiurnal lunar (M_2); however, the behavior of tides varies along the coast (Kantha, 2005). The southeast coastal system of the Gulf of Mexico is forced through its mouth by the mixed tide with a diurnal predominance regime, and loses this condition as it propagates toward the estuarine system. The main diurnal components in this system are K_1 and O_1, and the semidiurnal components are M_2 and N_2. The semidiurnal component S_2 is small at the mouth because there is an amphidromic point of M_2 and S_2 located in the middle of the Yucatan platform, where the area of minimum amplitude of S_2 is larger than that of M_2 (Kantha, 2005). Since S_2 is small at the mouth of the systems, its attenuation and dissipation takes place more quickly than the other two major components of the semidiurnal tide.

Spatial and temporal spectral features and harmonic analysis are used to describe the hydrodynamics of highly frictional coastal lagoons and tropical estuaries. In these systems, the balance between the pressure gradient and frictional forces control thetidal hydrodynamics. However, the frictional forces involved in the balance differ in each zone and within each system. Wind stress has a relative importance in the frictional force on some bodies of water along the coast of the Gulf of Mexico (Huang and Li, 2017), especially in the shallows and systems without small river discharge. Alvarado-Papaloapan is a good example of these systems. It includes the Camaronera lagoon, which is consistent with the tidal hydrodynamics of a “choked” coastal lagoon where the frictional forces that prevail in balance with the pressure gradient are the bottom friction and the morphological restrictions of the basin (Kjerfve and Magill, 1989; Hill, A. E., 1994; Fernandes *et al*, 2004, Tenorio-Fernández *et al*, 2016). On the other hand, the Limón and Papaloapan river zones (the area opposite to Camaronera lagoon in the Alvarado-Papaloapan system) are characterized by the freshwater discharge as a pulse in the opposite direction of the tides propagation and this force inhibits the propagation of the semidiurnal tide and in some cases of the diurnal signal (as in station L). This force fluctuates seasonally and is larger from May to October, during the biggest river fluxes. Therefore, it was necessary to analyze the propagation of the tide on a bimonthly basis to determine the seasonal variations of attenuation. Thus in addition to frictional forces, the opposite river pluses must be considered as an extra force which inhibit the tidal propagation in tropical estuaries.

The analytical method (explained above) was used for the bimonthly description of the tidal propagation along the longitudinal axis in a highly frictional tropical estuary. The analytical solution (equation (2)) is a function of a frictional parameter and follows Henrie and Valle-Levinson (2014) methodology to understand this parameter in each coastal body of water and therefore its frictional characteristics.

In the case of the Alvarado-Papaloapan estuary, the system was divided for its modeling into three zones according to its frictional characteristics: one that responds to the hydrodynamics of a highly frictional lagoon, *i.e*. the Alvarado zone; and the zones that display the same hydrodynamics plus the frictional forces derived of the discharge from rivers during the rainy season, *i.e.* the Limón and Papaloapan river zones, which can be considered as highly frictional estuaries. The analytical solutions resolve the amplitude, therefore the analytical model is considered a useful tool to describe the tidal amplitude propagation in a highly frictional estuary. However, not all phases are satisfactorily resolved, especially in the Alvarado zone, because the analytical and observation fit is in respect to the tidal amplitude only (Henrie and Valle-Levinson, 2014).

A common feature across the entire highly frictional semi-enclosed system with narrow and shallow mouths connected to the ocean is the energy peak of subtidal frequencies, which corresponds to periods longer than the inertial frequency (>38 hours). These signals may be produced by non-linear interactions between the main tidal components (“beats" or modulation frequency); by bottom friction, as usually observed in these kind of systems, (LeBlond, 1979; Hill, 1994); or by atmospheric forcing like winds, or extreme events as “Nortes” (extreme cold winds from the north) as well as river discharges. Huang and Li (2017) using in situ observations and numerical models in a coastal lagoon south of Louisiana reported high correlations between the extreme cold winds from the north and the subtidal variation of the water level and shows height correlation of remote atmospheric events and the local water level signal. Some similar correlation may happen in the subtidal signal of the Alvarado-Papaloapan estuary.

7. Conclusions

Tidal propagation in highly frictional estuaries can be described as the balance between the pressure gradient and the frictional forces, including the river pulses in the frictional term. Therefore, although river discharge show sub-tidal periodicity, river discharge has a strong influence on tidal hydrodynamics and inhibits the propagation of the tide toward the head within highly frictional estuarine systems.

In the Alvarado-Papaloapan estuary example, the Alvarado zone displays the characteristics of a semi-enclosed, highly frictional and shallow coastal lagoon on the western side. The Alvarado tidal hydrodynamics are driven by the balance between the pressure gradient and frictional forces due to the morphological restrictions of the basin and the friction with the bottom. On the eastern side, the areas influenced by the Limón and Papaloapan rivers show marked seasonal variations. These are characterized by a highly frictional and shallow estuary where tidal hydrodynamics is controlled by the same balance. However, the frictional forces are related to basin morphology, friction with the bottom, and river discharge, all are included in the frictional parameter δ.

8. Reference

Defant, A., 1958. Ebb and Flow. The tides of earth, air, and water. The University of Michigan Press, Ann Arbor, 121.

Emery, W. J., Thomson R. E., 2001. Data Analysis Methods in Physical Oceanography. Elsevier B. V., Amsterdam, 404-478.

Friedrichs, C. T., 2010. Barotropic tide in channelized estuaries. In: Valle-Levinson, A. (Eds.), Contemporary Issues in Estuarine Physics. Cambridge University Press, Cambridge, 27-61.

Godin, G., 1999. The propagation of tides up rivers with special considerations on the upper 401 Saint Lawrence River, Est. Coastal and Shelf Science. 48 (3), 307-324.

Henrie, K., Valle-Levinson, A., 2014. Sub-tidal variability in water levels inside a subtropical estuary. Journal of Geophysical Research 119, 7483-7492.

Hill, A. E., 1994. Fortnightly tide in a lagoon with variable choking. Estuarine, Coastal and Shelf Science 38, 423-434.

Huang, W., Li, C., 2017. Cold front driven flows through multiple inlets of Lake Pontchartrain Estuary. Journal of Geophysical Research: Oceans, 122 (11): 8627–8645.

Jay, D. A., (2010). Estuarine variability. In: Valle-Levinson, A. (eds.), Contemporary Issues in Estuarine Physics. Cambridge University Press, Cambridge, pp. 62-99.

Kantha, L., 2005. Barotropic Tide in the Gulf of Mexico. In: Circulation in the Gulf of Mexico Observation and Models. Geophysical Monograph Series 161, 159-16

Kjerfve, B., Magill, K., E., 1989. Geographic and hydrodynamic characteristics of shallow coastal lagoons. Marine Geology 88, 187-199.

LeBlond, P. H., 1978. On Tidal propagation in shallow rivers. Journal of Geophysical Research 86, 4717-4721.

LeBlond, P. H., 1979. Forced fortnightly tides in shallow rivers. Atmosphere-Ocean 17(3), 253-264.

Olvera-Prado, E. R., 2014. Hidrodinámica de la Laguna de Alvarado a partir de mediciones y modelación numérica. Posgrado en Ciencias de la Tierra, Centro de Ciencias de la Atmósfera, UNAM. Master thesis.

Pawlowicz, R., Beardsley, B., Lentz, S., 2002. Classical tidal harmonic analysis including error estimates in MATLAB using T_TIDE. Computers & Geosciences 28, 929-937.

Sassi, M., Hoitink A., 2013. River controls on tides and tide-mean water level profiles 432 in a tidal freshwater river, Journal Physical Oceanography: Oceans, 118 (9), 4139-4151.

Tenorio-Fernandez, L., Gomez-Valdes, J., Marino-Tapia, I., Enriquez C., Valle-Levinson, A., 2016. Tidal dynamics in a frictionally dominated tropical lagoon. Continental Shelf Research, (114) pp 16–28.

Torrence, C., & Compo, G. P. (1998). A practical guide to wavelet analysis. *Bulletin of the American Meteorological society*, *79*(1), 61-78.

Valle-Levinson, A., 2010. Definition and classification of estuaries. In: Valle-Levinson, A. (eds.), Contemporary Issues in Estuarine Physics. Cambridge University Press, Cambridge, pp. 1-11.

Van Rijn, L. C., (2011), Analytical and numerical analysis of tides and salinities in estuaries; part i: tidal wave propagation in convergent estuaries, Ocean Dyn., 61 (11), 1719-1741.

Waterhouse, A. F., Valle-Levinson, A., Winant, C. D., 2011. Tides in a system of connected estuaries. Journal of Physical Oceanography 41, 946-959, doi: 10.1175/2010JPO4504.1.

Winant, C. D., 2007. Three-dimensional tidal flow in an elongated, rotating basin. Journal of Physical Oceanography 37, 2345-2362.

Figure Captions

Fig. 1. Study area, zones that describe the sub-regions within the area and location of instruments in the lagoon-estuarine system.

Fig. 2. a) Time series of elevation anomaly of the water surface for all stations from 20 August to 20 September 2011, the mean of the whole times series was removed in each anomaly time series. Top panel, Alvarado zone, stations located at the mouth, station A and station B (head of Alvarado zone). Middle panel, Limón

river zone, from the mouth to station L. Bottom panel, Papaloapan river zone, from the mouth to station I. Location of sites are described in Fig. 1.

Fig. 3. Wavelet analysis in the station at the mouth (station J), the color bar is in (cm^2) x 10^4, left side. Right side, power spectrum density for the same station. Location of site is described in Fig. 1.

Fig. 4. Wavelet analysis for stations at Alvarado zone, the color bar is in (cm^2) x 10^4 (left side). Right side, power spectrum density for the same stations. The upper right part of the power spectrum density shows the station corresponding to the wavelet and the power spectrum density. Location sites are described in Fig 1.

Fig. 5. The top panel shows the average flow rate (m^3/s) of freshwater discharge from Limón river. The following panels show the wavelet analysis for stations on the Limón river zone sub-region, the color bar is in (cm^2) x 10^4; to the right, the power spectrum density for each station. Locations of sites are described in Fig.1.

Fig. 6. The top panel shows the average flow rate (m^3/s) of freshwater discharge from Papaloapan river. The bottom shows the wavelet analysis for the station on the Papaloapan river zone sub-region, the color bar is in (cm^2) x 10^4; to the right, the power spectra for that station. Locations of sites are described in Fig.1.

Fig. 7. Comparison between the normalized attenuation (a, b, and c), phases lags (d, e and f), the tidal diurnal main component O_1, and the data observed for diurnal signals (crosses) and semidiurnal signals (circles) in the Alvarado zone (a and d), Papaloapan river zone (b and e), and Limón river zone (c and f). Analytical solutions (N^0) along the longitudinal axis are represented by solid lines and dashed lines, according to the months and season (black lines are for winter months, blue lines are spring months and red lines are summer months). Phase lags are in degrees relative to the mouth for each zone. In all zones, both for standardized amplitude and for the phase-lag difference, the length relative to the mouth (axis x) was normalized using total length of the each zone, being zero at the mouth and one at end. The dashed lines in grey represent the normalized distance from the mouth (J) of the stations B, C, D, E, G, H, I and L (see Fig. 1).

Fig. 8. Comparison between the normalized attenuation (a, b, and c), phase lags (d, e and f), the tidal diurnal main component M_2, and the data observed for diurnal signals (crosses) and semidiurnal signals (circles) in the Alvarado zone (a and d), Papaloapan river zone (b and e), and Limón river zone (c and f). Analytical solutions (N^0) along the longitudinal axis are represented by solid lines and dashed lines, according to the months and seasons (black lines are for winter months, blue lines are spring months and red lines are summer months). Phase lags are in degrees relative to the mouth for each zone. In all zones, both for standardized amplitude and for the phase-lag difference, the length relative to the mouth (axis x) was normalized using total length of the each zone, being zero at the mouth and one at end. The dashed lines in grey represent the normalized distance from the mouth (J) of the stations B, C, D, E, G, H, I and L (see Fig. 1).

Legends to tables

Table 1. Zoning of the Alvarado-Papaloapan estuarine-lagoon system, geographic location of the sampling stations, sampling periods in each station, approximate sensor depth (h), approximate cross-section width (W), and approximate distance along axis from the mouth (L).

Table 2. Coefficient of Determination (R^2). Amplitude (A) and phase (θ) relative to the Greenwich meridian of the main tidal components for each station, amplitude-related error (δA), phase-related error ($\delta\theta$), signal-to-noice ratio (snr). Parameter figures are reported considering 95% confidence intervals. The name and location of each station are shown in Fig. 1.

Table 1

Sensor	Measurement period	h (~m)	W (~m)	L (~m)	Lon. W/ Lat. N
Mouth (J)	Aug 1 2011 - Dec 4 2011	4.31	1000	-----	95°45'14.3"/18° 46'10.2"
Alvarado zone					
Camaronera (A)	Aug 1 2011 - Sep 8 2012	1.13	4000	25000	95°56'42.8"/18°51' 27.4"
Buen País (B)	Aug 1 2011 - Aug 6 2012	1.15	2000	13000	95°52'11.2"/18°48'18.1"
Alvarado 1(C)	8 Dec 2011 - Sep 8 2012	1.01	5000	10000	95°50'05.9"/18°48'19.6"
Alvarado 2 (D)	8 Dec 2011 - Sep 9 2012	0.87	5000	10000	95°51'37.2"/18° 46'40.3"
Alvarado 3 (E)	8 Dec 2011 - Sep 9 2012	1.09	5000	8000	95°49'0.7"/18°47'46.1"
Limón river zone					
Tlalixcoyan (G)	Aug 2 2011- Sep 8 2012	1.09	3000	15000	95°51'45.5"/18°43'27.2"
Tlalix moth (H)	Aug 2 2011 - Sep 8 2012	1.12	600	8000	95°49'07.0"/18° 44'27.6"
Papaloapan (I)	Aug 2 2011 - Sep 9 2012	0.97	800		95°41'46.8"/18°44'04.2"
Limón (L)	Aug 10 2011 - Sep 8 2012	1.10	900	32000	95°52'31.7"/18°37'38.3"
Papaloapan river zone					
Acula (K)	Aug 11 2011 - Sep 8 2012	1.21	200	12000	95°46'10.0"/18°42'31.1"

Table 2

		Diurnal signal				Semidiurnal signal			
	R^2	O_1		K_1		M_2		N_2	
	(%)	A/θ	$\delta A/\delta\theta/snr$	A/θ	$\delta A/\delta\theta/snr$	A/θ	$\delta A/\delta\theta/snr$	A/θ	$\delta A/\delta\theta/snr$
(J)	71	13.5/18.1	0.7/22.5/380	12.3/22.5	0.7/3.3/310	7.8/252.1	0.2/6.3/110	2.1/239.8	0.7/22.5/380
Alvarado zone									
(E)	65	11.0/39.0	0.2/0.9/410	10.7/43.5	0.2/0.9/390	6.0/287.7	0.1/0.8/560	1.3/274.5	0.1/3.4/270
(D)	68	10.9/39.0	0.2/1.0/360	10.7/45.6	0.2/1.0/340	6.0/288.3	0.1/0.1/370	1.3/276.1	0.1/4.3/170
(C)	53	11.0/39.0	0.2/1.1/330	10.8/43.9	0.2/1.1/310	6.1/288.1	0.1/0.1/480	1.3/274.6	0.1/3.7/230
(B)	63	10.3/44.1	0.2/1.3/210	10.0/52.9	0.2/1.3/210	5.7/290.0	0.1/4.1/190	1.3/290.0	0.1/4.1/190
(A)	30	2.1/106.6	0.1/3.2/350	1.7/114.6	0.1/1.3/240	-------	-------	-------	-------
Limón river zone									
(H)	58	9.6/42.4	0.1/0.1/450	9.5/50.1	0.1/0.1/440	5.2/297.1	0.1/0.1/540	1.1/285.9	0.1/3.6/250
(G)	46	8.6/47.2	0.1/0.1/380	8.6/57.8	0.1/0.1/380	4.8/310.2	0.1/0.1/390	1.0/300.0	0.1/4.3/170
(L)	51	2.1/96.3	0.1/0.1/100	2.1/114.0	0.2/5.7/110	-------	-------	-------	-------
(K)	52	7.2/59.1	0.1/1.1/280	7.1/66.0	0.1/1.1/270	3.2/315.6	0.1/0.1/620	-------	-------
Papaloapan river zone									
(I)	67	11.2/30.2	0.2/1.3/210	11.3/35.0	0.2/1.3/210	6.4/277.5	0.1/0.9/340	1.5/258.8	0.1/3.8/230

Through wavelets, power spectral density and using a linear analytical model, the tidal and river interactions were described.

One year of water level observations in the tropical estuarine were obtained from eleven measuring stations.

The high attenuation in the estuary zone shows temporal variations.

The river discharges are added to frictional forces in the tidal propagation analytical model.

Rivers seasonal variable discharges have a strong influence on tidal hydrodynamics and inhibit the propagation of tides.

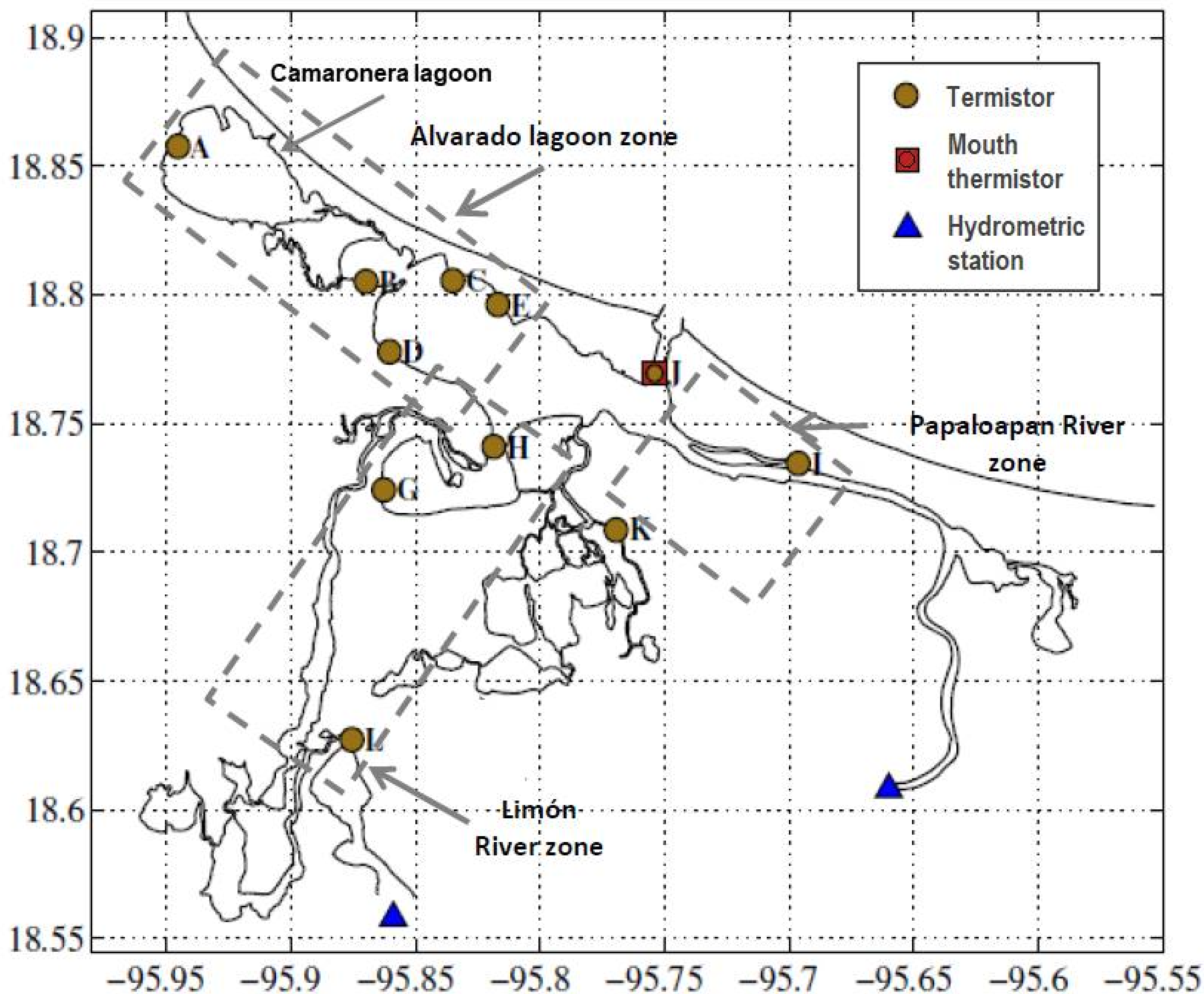

Camaronera lagoon
Alvarado lagoon zone
Papaloapan River zone
Limón River zone
Termistor
Mouth thermistor
Hydrometric station
A
B
C
D
E
G
H
I
J
K
L
18.9
18.85
18.8
18.75
18.7
18.65
18.6
18.55
−95.95
−95.9
−95.85
−95.8
−95.75
−95.7
−95.65
−95.6
−95.55

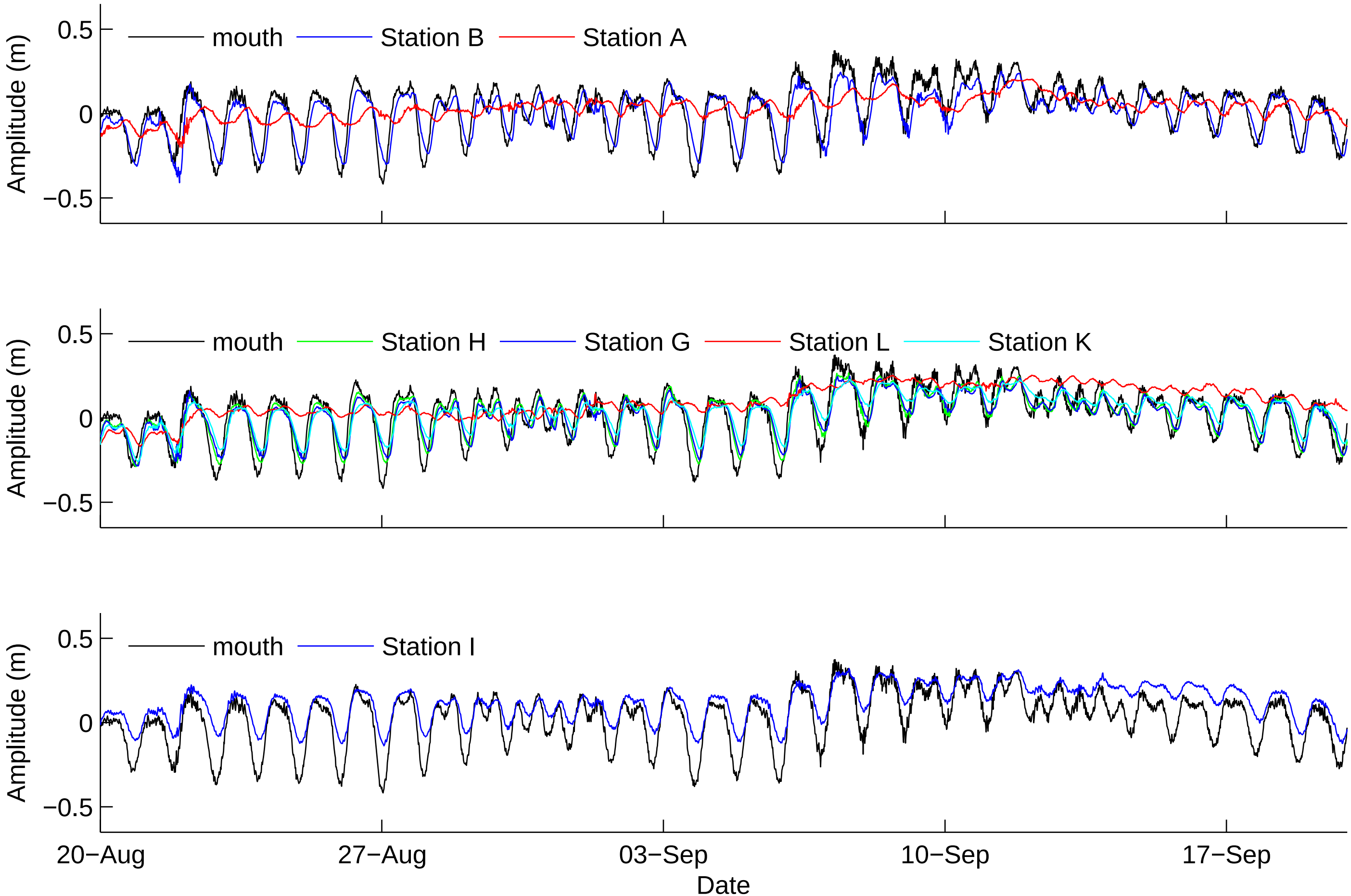

Amplitude (m)
0.5
0
−0.5
mouth
Station B
Station A
Amplitude (m)
0.5
0
−0.5
mouth
Station H
Station G
Station L
Station K
Amplitude (m)
0.5
0
−0.5
mouth
Station I
20−Aug
27−Aug
03−Sep
10−Sep
17−Sep
Date

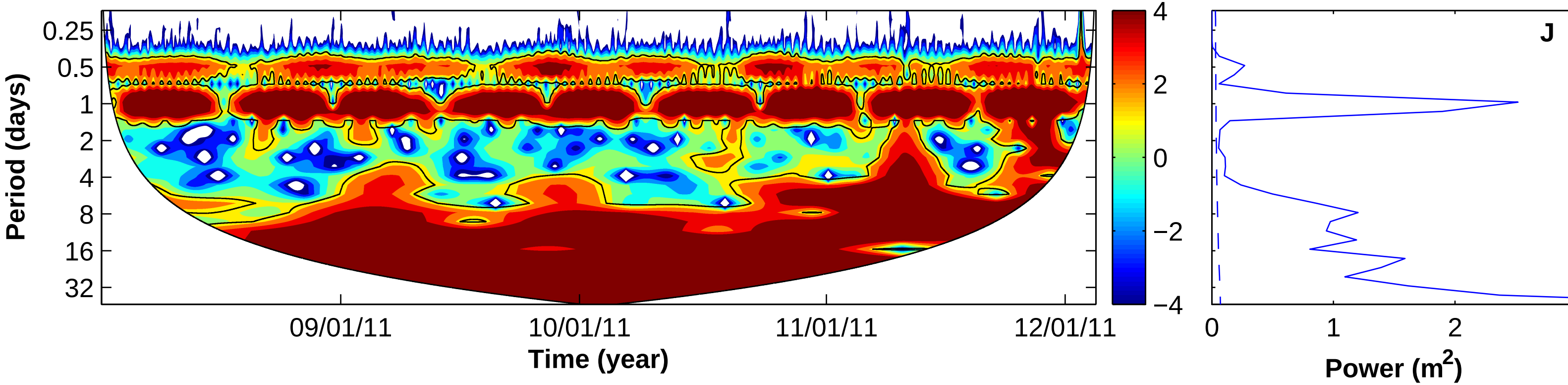

0.25
0.5
1
2
4
8
16
32
Period (days)
09/01/11
10/01/11
11/01/11
12/01/11
Time (year)
4
2
0
−2
−4
J
0
1
2
3
Power (m2)

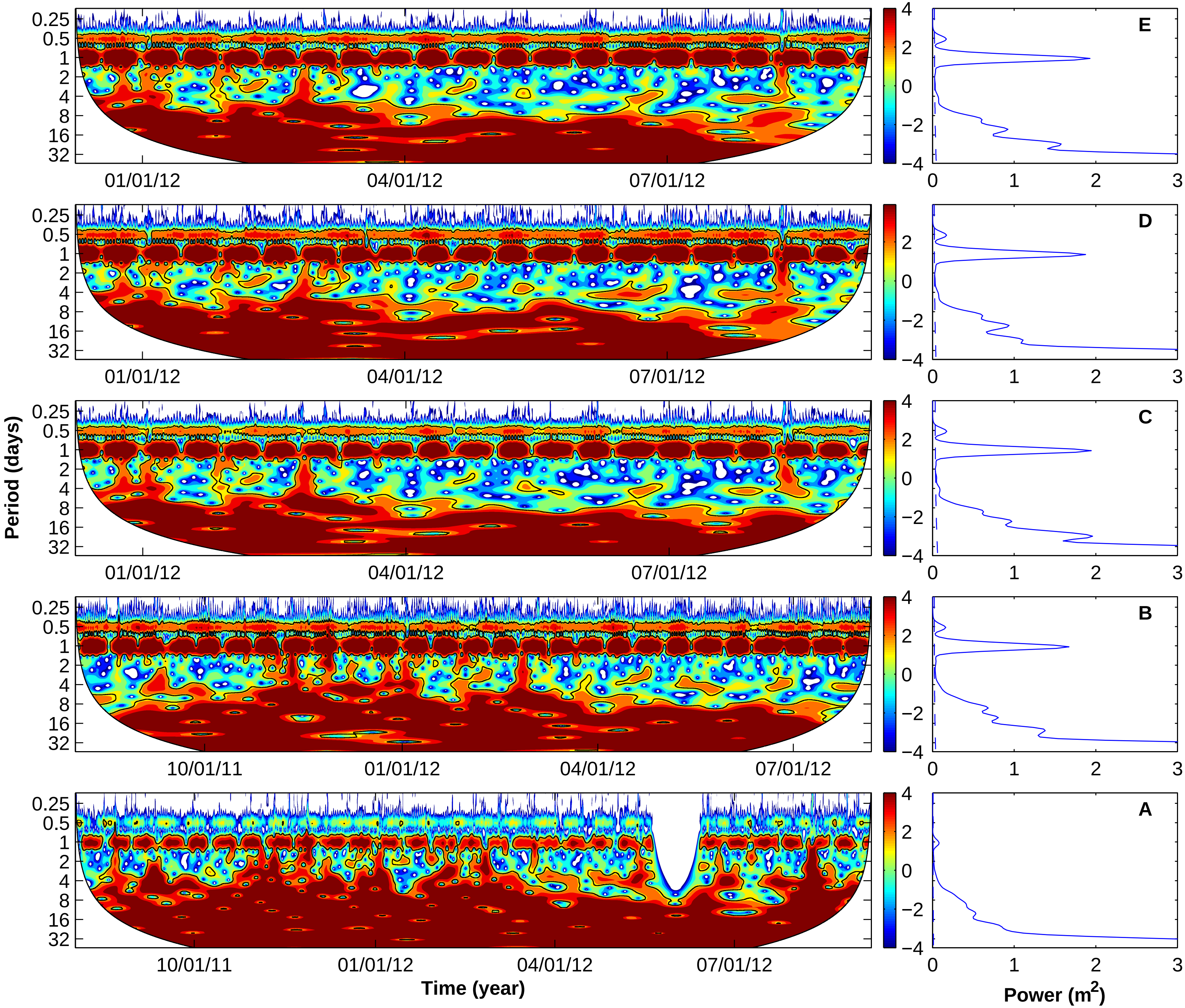
E
D
C
B
A
Period (days)
0.25
0.5
1
2
4
8
16
32
01/01/12
04/01/12
07/01/12
10/01/11
Time (year)
Power (m^2)
4
2
0
−2
−4
0
1
2
3

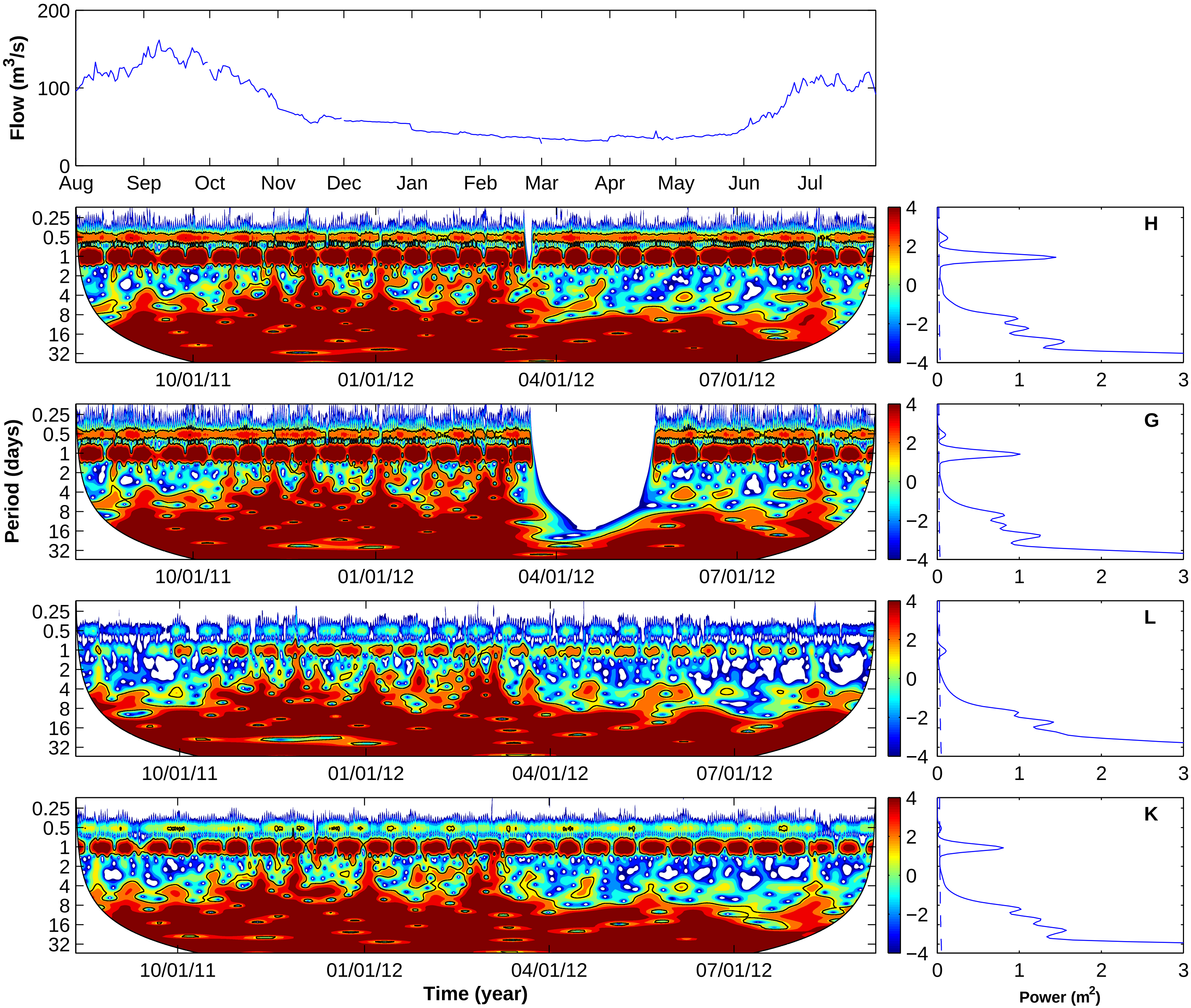

Flow (m3/s)
200
100
0
Aug
Sep
Oct
Nov
Dec
Jan
Feb
Mar
Apr
May
Jun
Jul
Period (days)
0.25
0.5
1
2
4
8
16
32
10/01/11
01/01/12
04/01/12
07/01/12
H
G
L
K
4
2
0
−2
−4
0
1
2
3
Time (year)
Power (m2)

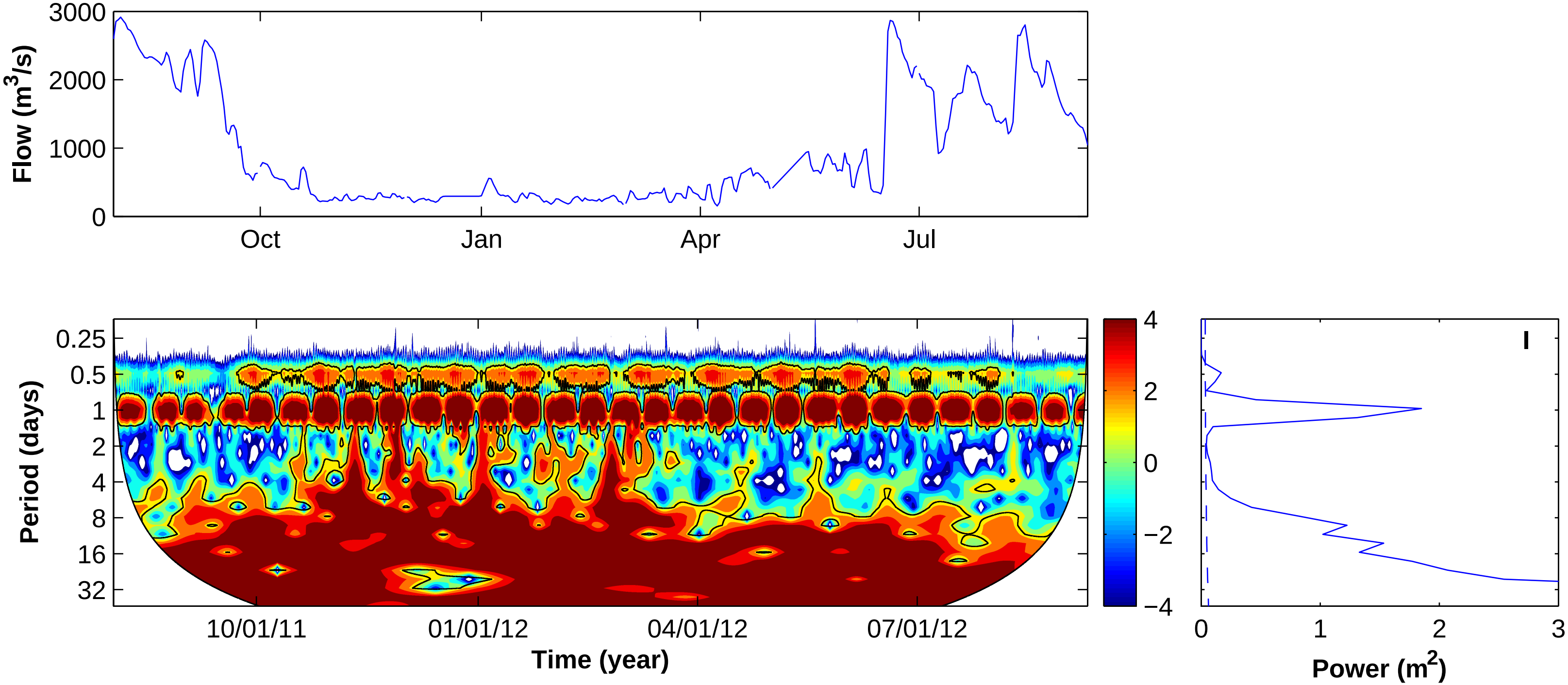
3000
2000
1000
0
Flow (m3/s)
Oct
Jan
Apr
Jul
0.25
0.5
1
2
4
8
16
32
Period (days)
10/01/11
01/01/12
04/01/12
07/01/12
Time (year)
4
2
0
−2
−4
I
0
1
2
3
Power (m2)

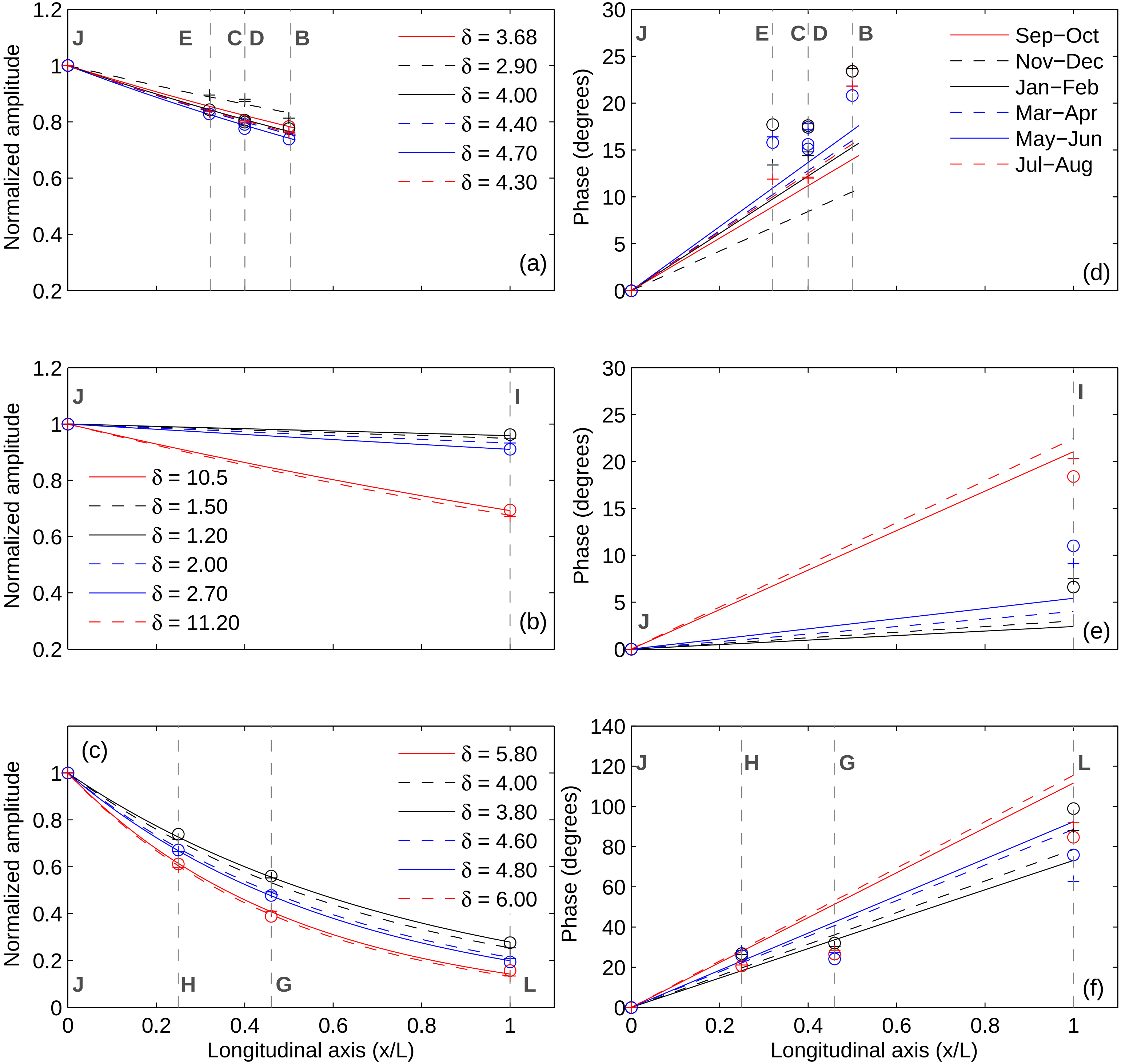

δ = 3.68
δ = 2.90
δ = 4.00
δ = 4.40
δ = 4.70
δ = 4.30
(a)
Sep−Oct
Nov−Dec
Jan−Feb
Mar−Apr
May−Jun
Jul−Aug
(d)
δ = 10.5
δ = 1.50
δ = 1.20
δ = 2.00
δ = 2.70
δ = 11.20
(b)
(e)
δ = 5.80
δ = 4.00
δ = 3.80
δ = 4.60
δ = 4.80
δ = 6.00
(c)
(f)
J
E
C
D
B
I
H
G
L
Normalized amplitude
Phase (degrees)
Longitudinal axis (x/L)

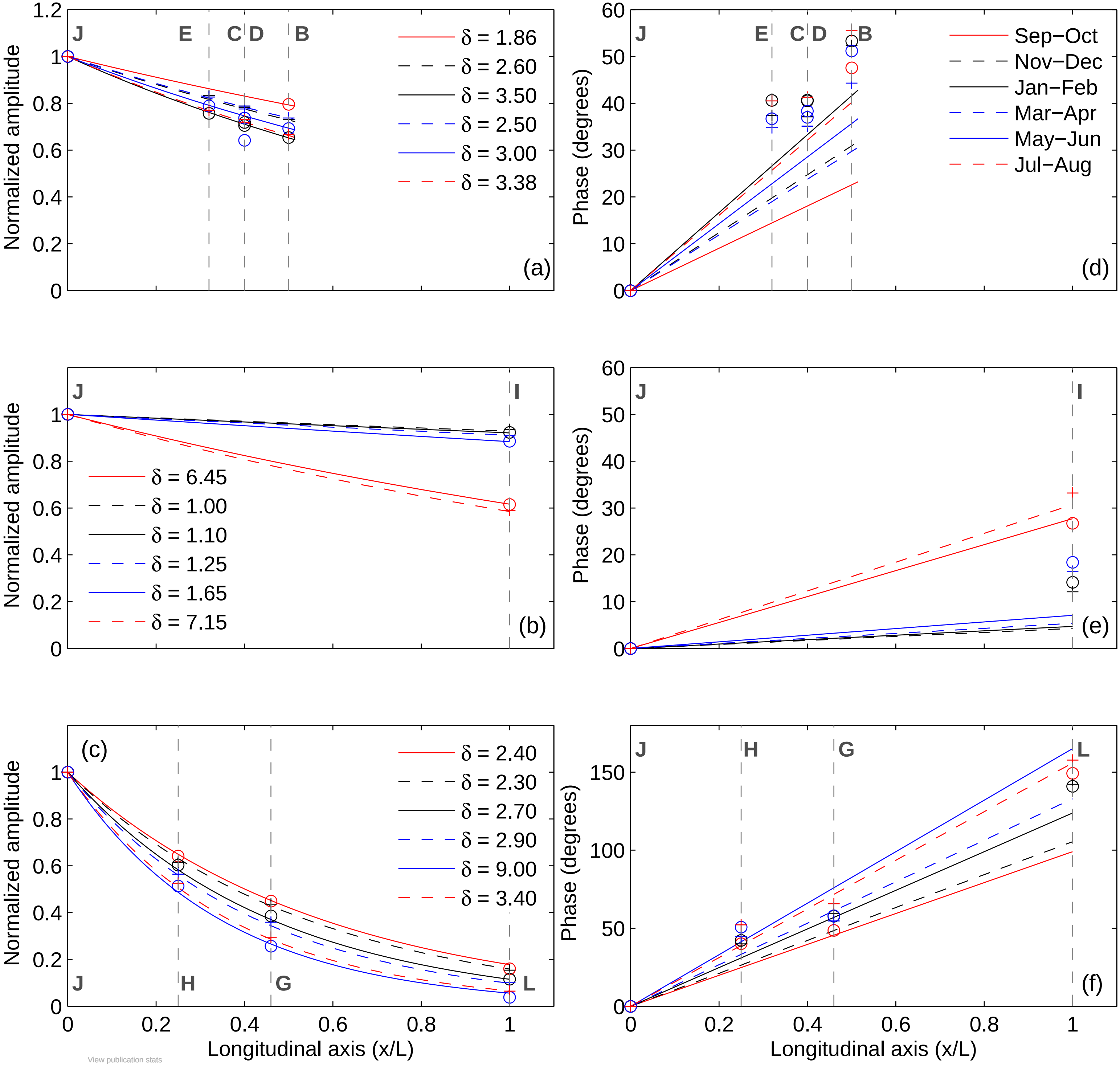
(a)
(b)
(c)
(d)
(e)
(f)
Normalized amplitude
Phase (degrees)
Longitudinal axis (x/L)
J
E
C
D
B
I
H
G
L
δ = 1.86
δ = 2.60
δ = 3.50
δ = 2.50
δ = 3.00
δ = 3.38
δ = 6.45
δ = 1.00
δ = 1.10
δ = 1.25
δ = 1.65
δ = 7.15
δ = 2.40
δ = 2.30
δ = 2.70
δ = 2.90
δ = 9.00
δ = 3.40
Sep−Oct
Nov−Dec
Jan−Feb
Mar−Apr
May−Jun
Jul−Aug